



Assessing Mechanochemical Properties of Acrylonitrile Butadiene Styrene (ABS) Items in Cultural Heritage Through a Multimodal Spectroscopic Approach

Journal:	<i>Applied Spectroscopy</i>
Manuscript ID	ASP-24-0116.R1
Manuscript Type:	Special Issue
Date Submitted by the Author:	23-May-2024
Complete List of Authors:	Bargagli, Irene; CNR, Istituto di Scienze e Tecnologie Chimiche "Giulio Natta" Alunni Cardinali, Martina; University of Perugia, Chemistry, Biology and Biotechnology Di Tullio, Valeria; CNR, Istituto di Scienze del Patrimonio (ISPC) Doherty, Brenda; CNR, Istituto di Scienze e Tecnologie Chimiche "Giulio Natta" Paolantoni, Marco; Universita degli Studi di Perugia, Chimica, Biologia e Biotecnologie Fioretto, Daniele; University of Perugia, Physics and Geology Proietti, Noemi; CNR, Istituto di Scienze del Patrimonio (ISPC) Sabatini, Francesca; CNR, Istituto di Scienze e Tecnologie Chimiche "Giulio Natta" (SCITEC) Miliani, Costanza ; CNR, Istituto di Scienze del Patrimonio (ISPC) Storace, Elisa; Kartell SpA, Kartell Museum Russo, Sara; Università degli Studi di Firenze, Dipartimento di Storia, Archeologia, Geografia, Arte e Spettacolo Trevisan, Rafaela; Fondazione La Triennale di Milano, Conservazione e restauro Vannini, Alessandra; Fondazione La Triennale di Milano, Conservazione e restauro Cartechini, Laura; CNR, Istituto di Scienze e Tecnologie Chimiche "Giulio Natta" (SCITEC) Comez, Lucia; CNR, Istituto Officina dei Materiali (IOM) Rosi, Francesca ; CNR, Istituto di Scienze e Tecnologie Chimiche "Giulio Natta" (SCITEC)
Manuscript Keywords:	Brillouin micro-spectroscopy, Raman micro-spectroscopy, external reflection IR spectroscopy, NMR relaxometry, photoaging
Abstract:	A multimodal spectroscopic approach is proposed to correlate the mechanical and chemical properties of plastic materials in art and design objects, at both surface and sub-surface levels, to obtain information about their conservation state and to monitor their degradation. The approach was used to investigate the photooxidation of Acrylonitrile-Butadiene-Styrene (ABS), a plastic commonly found in many artistic and design applications, using ABS-based LEGO® bricks as model samples. The modifications of the chemical and viscoelastic properties of ABS during photoaging were monitored by correlative Brillouin and Raman micro-spectroscopy (BRaMS), combined with portable and noninvasive broad range external reflection IR spectroscopy and NMR relaxometry,

1
2
3
4
5
6
7
8
9
10
11
12
13
14
15
16
17
18
19
20
21
22
23
24
25
26
27
28
29
30
31
32
33
34
35
36
37
38
39
40
41
42
43
44
45
46
47
48
49
50
51
52
53
54
55
56
57
58
59
60

	<p>directly applicable in museums. BRaMS enabled combined measurements of Brillouin light scattering (BLS) and Raman spectroscopy in a micro-spectroscopic setup, providing for the coincident probe of the chemical and mechanical changes of ABS at the sample surface. NMR relaxometry allowed for noninvasive measurements of relaxation times and depth profiles which are directly related to the molecular mobility of the material. Complementary chemical information was acquired by external reflection IR spectroscopy. The simultaneous probe of the chemical and mechanical properties by this multimodal spectroscopic approach enabled us to define a decay model of ABS in terms of compositional changes and variation of stiffness and rigidity occurring with photodegradation. The knowledge acquired on LEGO® samples has been used to rate the conservation state of ABS design objects non-invasively investigated by external reflection FTIR spectroscopy and NMR relaxometry offered by the MOLAB platform of the European Research Infrastructure of Heritage Science-ERIHS.</p>

SCHOLARONE™
Manuscripts

Paper Type: *Submitted Manuscript for VISPEC Special Issue*

Colour Figures in Print?: YES; colour figures in print, as well as online

Assessing Mechanochemical Properties of Acrylonitrile Butadiene Styrene (ABS) Items in Cultural Heritage Through a Multimodal Spectroscopic Approach

Irene Bargagli^{1,2,#}, Martina Alunni Cardinali^{2,#}, Valeria Di Tullio³, Brenda Doherty¹, Marco Paolantoni², Daniele Fioretto^{4,5}, Noemi Proietti³, Francesca Sabatini^{1†}, Costanza Miliani⁶, Elisa Storage⁷, Sara Russo⁸, Rafaela Trevisan⁹, Alessandra Vannini⁹, Laura Cartechini^{1,*}, Lucia Comez^{5,*}, Francesca Rosi^{1,*}

authors contributed equally

¹ CNR, Istituto di Scienze e Tecnologie Chimiche “Giulio Natta” (SCITEC), via Elce di Sotto, 8 06123 Perugia, Italy

² Department of Chemistry, Biology and Biotechnology, University of Perugia via Elce di Sotto, 8 06123, Italy

³ CNR, Istituto di Scienze del Patrimonio (ISPC), Strada Provinciale 35d, n. 9, 00010, Montelibretti (Roma), Italy

⁴ Dipartimento di Fisica e Geologia Università di Perugia, via Pascoli 8 06123 Perugia

⁵ CNR, Istituto Officina dei Materiali (IOM), Via Pascoli, 06123 Perugia, Italy

⁶ CNR, Istituto di Scienze del Patrimonio (ISPC), Via Guglielmo Sanfelice, 8 80134 Napoli, Italy

⁷ Fondazione Museo Kartell, Via delle Industrie 3, 20082 Noviglio Milano, Italy

⁸ Università degli Studi di Firenze, Dipartimento di Storia, Archeologia, Geografia, Arte e Spettacolo, Via S. Gallo, 10-50129 Firenze, Italy

⁹ Triennale Milano, Conservazione e restauro, viale Emilio Alemagna 6, 20121 Milano, Italy

† Present address: Department of Earth and Environmental Sciences, University of Milano-Bicocca, Piazza della Scienza 1, 20126 Milan, Italy

*Corresponding author emails: laura.cartechini@cnr.it; comez@iom.cnr.it; francesca.rosi@cnr.it

Abstract

A multimodal spectroscopic approach is proposed to correlate the mechanical and chemical properties of plastic materials in art and design objects, at both surface and sub-surface levels, to obtain information about their conservation state and to monitor their degradation. The approach was used to investigate the photooxidation of acrylonitrile butadiene styrene (ABS), a plastic commonly found in many artistic and design applications, using ABS-based LEGO bricks as model samples. The modifications of the chemical and viscoelastic properties of ABS during photoaging were monitored by correlative Brillouin and Raman microspectroscopy (BRaMS), combined with portable and noninvasive broad range external reflection IR spectroscopy and nuclear magnetic resonance (NMR) relaxometry, directly applicable in museums. BRaMS enabled combined measurements of Brillouin light scattering (BLS) and Raman spectroscopy in a micro-spectroscopic setup, providing for the coincident probe of the chemical and mechanical changes of ABS at the sample surface. NMR relaxometry allowed for noninvasive measurements of relaxation times and depth profiles which are directly related to the molecular mobility of the material. Complementary chemical information was acquired by external reflection infrared (IR) spectroscopy. The simultaneous probe of the chemical and mechanical properties by this multimodal spectroscopic approach enabled us to define a decay model of ABS in terms of compositional changes and variation of stiffness and rigidity occurring with photodegradation. The knowledge acquired on LEGO samples has been used to rate the conservation state of ABS design objects non-invasively investigated by external reflection Fourier transform infrared (FT-IR) spectroscopy and NMR relaxometry offered by the MOBILE LABORATORY (MOLAB) platform of the European Research Infrastructure of Heritage Science (ERIHS).

Keywords

Brillouin microspectroscopy, Raman microspectroscopy, external reflection infrared spectroscopy, nuclear magnetic resonance relaxometry, NMR relaxometry, photoaging

Introduction

Plastic was firmly established as an essential component of daily life in the 1960s. Due to its unrivalled versatility, it has succeeded in a variety of sectors, from toys, automotive parts, and food packaging to design and arts, providing a versatile medium for the artistic expression of designers and artists akin.¹ Among the numerous materials encountered in the realm of art and

1
2
3 design, acrylonitrile butadiene styrene (ABS) has gained popularity due to its extensive use in
4 crafting various artifacts.
5

6 ABS is composed of a continuous phase of acrylonitrile–styrene (SAN, the glassy matrix)
7 and a dispersed phase of partially grafted polybutadiene (PB, the rubbery phase).² This unique
8 configuration imparts distinctive properties to ABS, including high impact resistance,
9 mechanical strength, and excellent moldability. Due to its desirable characteristics, ABS has
10 become a preferred choice for artists and designers, leading to its extensive use in sculptures,
11 decorative pieces, and everyday objects^{3,4} as well as a rapid prototyping material. It is therefore
12 expected to remain present in museums and collections for many years to come.⁵
13
14
15
16
17
18

19 There is extensive literature on the degradation issues of ABS by exposure to heat or
20 light, which mainly induces radical oxidation of the PB component. This leads to a decrease in
21 the double bond content, followed by cross-linking of the PB oxidized phase. Prolonged aging
22 gives rise to further chain scission reactions with depolymerization of the SAN fraction. These
23 chemical modifications translate into significant alterations of the mechanical properties of the
24 materials.^{6–11} Over time, this can result in reduced strength, toughness, and flexibility of ABS. In
25 cultural heritage preservation, monitoring the degradation provides valuable insights into the
26 material's long-term durability. Early detection of degradation enables preventive conservation
27 measures to be aptly taken, such as adjusting display conditions or implementing protective
28 coatings. These actions slow down or prevent further deterioration, safeguarding the objects.
29 The availability of samples allows the exploitation of a wide range of techniques for polymer
30 analysis, both for compositional identification and the study of ABS stability.¹² Techniques such
31 as thermogravimetric analysis (TGA) coupled with Fourier transform infrared (FT-IR) or mass
32 spectrometry (MS), differential scanning calorimetry (DSC), and evolved gas analysis coupled
33 with mass spectrometry (EGA-MS), as well as pyrolysis coupled with gas chromatography and
34 mass spectrometry (Py-GC-MS), and combinations have been employed.¹¹
35
36
37
38
39
40
41
42
43
44
45

46 Regarding spectroscopic techniques, the most used in polymer analysis is Fourier
47 transform infrared spectroscopy (FT-IR), particularly in the attenuated total reflection (ATR)
48 modality, which has been successful in identifying plastics and additives in collections.^{13–16}
49 However, in recent decades, cultural heritage analytical approaches have shifted towards entirely
50 non-invasive methodologies, recognizing the importance of preserving irreplaceable artifacts
51 avoiding sampling. Traditional micro-destructive techniques, although minimal, can still pose
52
53
54
55
56
57
58
59
60

1
2
3 risks to these precious objects and have limited representativeness. Consequently, there is an
4 increasing demand for innovative approaches that enable the study of cultural heritage materials
5 without any contact with the object's surface.
6
7

8 External reflection infrared spectroscopy in the mid and near IR spectral ranges^{3,17–21}
9 (8000–400 cm⁻¹) is a powerful technique currently used for noninvasive and noncontact
10 chemical analysis of the surface and subsurface composition of heritage plastic materials. This
11 technique enables the identification of polymers estimating the relative monomer composition in
12 blends and provides spectral markers for plastic degradation.^{3,22,23} Raman spectroscopy is, also,
13 extensively exploited to these aims, as reported in recent literature.^{24–26}
14
15
16
17

18 Driven by the need to expand the understanding of the conservation status of plastic
19 design items, a noninvasive multimodal spectroscopic approach is proposed herein, capable of
20 correlating the chemical and mechanical changes that occur with aging, going beyond the
21 identification of plastics.
22
23
24

25 Specifically, in situ external reflection IR spectroscopy has been combined with portable
26 NMR-relaxometry (thus probing the surface and subsurface polymer composition and mobility)
27 and correlative Brillouin and Raman microspectroscopy (BRaMS, available as laboratory set up).
28
29
30

31 Nuclear magnetic resonance (NMR) relaxometry is a noninvasive inspection technique
32 well consolidated in heritage science that can be performed in situ. It provides information on
33 proton spin density and relaxation times (mobility) in function of depth, down to a few mm with
34 micrometric spatial resolution.^{27,28}
35
36
37

38 BRaMS is a novel technique that has only recently been applied in the field of heritage
39 science.²⁹ It enables combined measurements of Brillouin light scattering (BLS) and Raman
40 spectroscopy in a micro-spectroscopic setup, providing the simultaneous spatially resolved
41 monitoring of the chemical and mechanical changes occurring at the sample surface.^{30,31}
42 Brillouin spectrum results from the interaction of light with thermally activated acoustic waves
43 (phonons) traveling in the sample and thus characterizes the collective modes of the material,
44 from which its longitudinal elastic modulus (M) can be derived. Moreover, it probes mechanical
45 properties without any external perturbations of the system and operates in the gigahertz range,
46 inaccessible by traditional tensile testing. BRaMS integrates the BLS analysis with
47 compositional information obtained through Raman simultaneously performed on the same
48 point.
49
50
51
52
53
54
55
56
57
58
59
60

1
2
3 LEGO bricks made of ABS were chosen due to their low cost and availability and
4 subjected to photochemical aging through light exposure. The aims were twofold: (i) to correlate
5 chemical and viscoelastic (mechanical) changes due to photodegradation of ABS, and (ii) to
6 propose a multimodal approach for in situ assessment of the state of conservation of historical
7 plastic objects.
8
9

10
11 The mechanochemical correlation derived from the study of the photoaged LEGO was
12 employed to interpret noninvasive data obtained in situ by external reflection IR spectroscopy
13 and NMR relaxometry on plastic design items made of ABS conserved at the Italian Design
14 Museum and Kartell Museum and to evaluate their conservation state. The in situ noninvasive
15 investigations were performed within the access activity of the MOBILE LABORATORY (MOLAB)
16 platform of the Italian node of the European Research Infrastructure for Heritage Science (E-
17 RIHS).³²
18
19
20
21
22
23
24

25 **<COPYED/TYPESET>Please use title case ONLY for H3 headings, do not remove period**
26 **between heading and start of sentence. Please use the guidelines for formatting Heading #3**
27 **(<H3></H3>) as noted throughout and outlined in the ASP style sheet, e.g., "Lightface,**
28 **italic, cap and lowercase, reverse italic used, text run-in; no semi-colon or colon".**
29
30

31 **</COPYED/TYPESET>**
32

33 **Experimental**

34 *Materials and Methods*

35
36 **<H3>Samples.</H3>** A set of LEGO bricks (The Lego Group) in lime green colour was
37 purchased from a local store in Italy in July 2022 (batch number 11019). The samples contained
38 titanium dioxide (TiO₂) as filler and phthalocyanine pigments (Pigment Green 7–PG7 and
39 Pigment Green 36–PG36).¹¹ A second set of LEGO bricks in lime green colour (ID element
40 4165967, ID design 3001) was bought online from the official LEGO website in February 2023.
41 The two sets of LEGO bricks were artificially aged using a Cermax filtered Xenon lamp (300 W,
42 $\lambda > 320$ nm), placing the bricks at 50 cm from the light source. The temperature during the
43 irradiation was approximately 30<thinspace>°C, with variation below 10%.**<AUTHOR>Please**
44 **note that all instances of "ca." were replaced with "approximately" due to the fact that ca.**
45 **is applied only to time in the journal. Managing Editor</AUTHOR>** The ABS chemical–
46 physical properties were monitored at different stages of light aging, expressed in energy density
47
48
49
50
51
52
53
54
55
56
57
58
59
60

1
2
3 units or dose (kJ/cm^2) as calculated by spectro-radiometric measurements (irradiance, $\Phi_0 = 60$
4
5
6 W/m^2 , and illuminance, $E_{m0} = 40.980$ lux for the set 2022 and irradiance, $\Phi_0 = 80$ W/m^2 , and
7
8 illuminance, $E_{m0} = 54.64$ lux for the set 2023) for a total time of 437 and 525 hours for the sets
9
10 of 2022 and 2023, respectively.
11

12
13 **<H3>Historical Design Objects.</H3>** The studied objects were a selection of ABS plastic
14
15 artworks belonging to the Italian Design Museum and the Kartell Museum. The results presented
16
17 here refer to the objects depicted in Figure S1 (Supplemental Material), i.e., Grillo Phone-0061,
18
19 Divisumma-0336, and Componibile-4955.
20

21
22 **<H3>External Reflection FT-IR Spectroscopy.</H3>** The Bruker Optics ALPHA-R
23
24 spectrophotometer is equipped with a SiC Globar infrared radiation source, a Michelson
25
26 interferometer (RockSolid design, Bruker Optics) and a room temperature deuterated L-alanine
27
28 doped tri-glycine sulfate (DLaTGS) detector. The optical layout is $22^\circ/22^\circ$, collecting the
29
30 infrared radiation reflected from a surface located at about 1 cm distance from the external
31
32 reflection module and the probed area is about 6 mm in diameter. The investigated area is
33
34 visualized by the USB video camera. External reflection-mode spectra, expressed as pseudo-
35
36 absorbance $A' = \log(1/R)$; $R =$ reflectance, were recorded in the range $8000\text{--}400$ cm^{-1} using a gold
37
38 mirror plate as background with a spectral resolution is 4 cm^{-1} and acquiring 186 scans.
39

40
41 The photochemical aging was followed by monitoring the ratio of the integrated areas of
42
43 PB bands at 965 cm^{-1} $\delta(\text{CH})_{\text{trans}}$ and at 4480 cm^{-1} $(\nu + \delta)\text{CH}$, performing three measurements for
44
45 each brick. The two selected bands allow to probe the consumption of the PB phase at the
46
47 surface of the sample with respect to the subsurface composition, exploiting the different
48
49 penetration depth of the IR light in the mid- and near IR-range for the two vibrational modes (the
50
51 first microns and the latter approximately hundreds of mm, respectively).³
52

53
54 Before integration, Kramers–Kronig transformation (available in the software IR-OPUS
55
56 Base Package) was applied in the range $1000\text{--}600$ cm^{-1} to correct the band of PB at 965 cm^{-1}
57
58 when appearing as a derivative-like band due to Fresnel type reflection.³³
59
60

Finally, the 965 cm^{-1} to 4480 cm^{-1} band ratio decrease with respect to the energy dose was fitted using a one-phase exponential decay function, and its value was considered as a surface degradation index (SDI) value (Eq. 1):

$$\text{SDI} = 66e^{-\left(\frac{\text{energy}}{7.29}\right)} \quad (1)$$

The SDI parameter is an estimation of the photodegradation progression acting on the ABS surface and can be used to evaluate the energy per unit area that ran over the object.

Brillouin and Raman Microspectroscopy. The Brillouin and Raman microspectroscopy experiment consists of a combined setup in which the light from a 532 nm single-mode solid-state laser is focused on the sample surface by a microscope objective. The backscattered light is then split in frequency and direction by an edge filter so that the Stokes component ($>30\text{ cm}^{-1}$) is sent to a Horiba iHR320 Triax Raman monochromator, and the quasi-elastic and anti-Stokes components ($<30\text{ cm}^{-1}$) are sent to a high-contrast multipass tandem Fabry–Perot interferometer (TFP-2 HC, JRS Scientific Instruments) for simultaneous Raman and Brillouin analysis. The sample is mounted on an x,y,z translation stage for single-point and mapping experiments, the details of which are discussed in Scarponi et al.³⁰ Each Brillouin–Raman spectrum was collected for approximately $2 \times 60\text{ s}$ using a 600 lines/mm grating and a $100\text{ }\mu\text{m}$ slit aperture. Laser power at the sample was set to $<1\text{ mW}$ to avoid local photodamage. A microscope objective $20\times$ (NA=0.42) was chosen for the analysis because its coupling with the green laser source allows a very localized analysis of the sample surface (axial resolution of about $10\text{ }\mu\text{m}$). Considering the optical setup and measuring conditions, each surface point was exposed to an energy dose $\leq 38.2\text{ mJ}/\mu\text{m}^2$. The reported BRaMS profiles are an average of five spectra acquired randomly on the samples surface.

Unilateral NMR. The NMR measurements were performed at 17.6 MHz ^1H resonance frequency (RF) using an NMR mobile universal surface explorer (NMR-MOUSE) from Bruker Biospin interfaced with a single-sided sensor by Rheinisch Westfälische Technische Hochschule (RWTH), Aachen University (Germany).³⁴ This sensor generates, in the probed area ($15 \times 20\text{ mm}^2$) and 3 mm away from the radiofrequency (RF) coil, a magnetic field of around

0.411 T, with an extremely uniform gradient G of 20 Tm^{-1} along the depth direction and a $\pi/2$ pulse of $4 \mu\text{s}$ to resolve the near surface structure of arbitrary large samples. Measurements of the two processes of magnetization decay, described by the time constants T_1 and T_2 respectively, were recorded from the surface (0.2 mm) and extended up to 1.9 mm inside the sample at intervals of $100 \mu\text{m}$, maintaining a spatial resolution of around $50 \mu\text{m}$. However, within the range of 0 to 0.1 mm, the signal-to-noise ratio (S/N) was found to be too noisy to perform any significant fit. Spin-spin or transverse relaxation decay, T_2 , was acquired using Carr-Purcell-Meiboom-Gill (CPMG) pulse sequence, with an echo-time (TE) of $34 \mu\text{s}$, an acquisition time of $6 \mu\text{s}$, 2048 echoes, and a recycle delay of 0.4 s to provide the optimum S/N and to optimize the CPMG decay curve. The magnetic field of the NMR-MOUSE is highly inhomogeneous, indicating that RF pulses are disrupted by resonance offsets within the selected volume. This also leads to the echo decay from the CPMG sequence only approximating the decay in a uniform magnetic field, and the T_2 relaxation times are in this instance referred to as $T_{2\text{eff}}$. The distribution of T_2 was obtained by applying an UPEN algorithm (Matlab) to the echo train recorded by the CPMG pulse sequence. Spin-lattice or longitudinal relaxation decay, T_1 , was acquired by applying a saturation recovery pulse sequence. The experimental data of longitudinal decay were fit according to the following equation (Eq. 2):

$$f(t) = C_0 + \sum_{i=1}^n W_i \exp\left(-\frac{t}{T_{1i}}\right) \quad (2)$$

where n is the number of components of the decay of the magnetization, W_i is the weight of the i th component, C_0 is the offset value which accounts for the noise of the measurement, and T_{1i} is the relaxation time of the i th component.

Results and Discussion

Mechanochemical Study of ABS-Based LEGO Bricks

Figure 1a depicts the three repeating units composing the ABS polymer: polyacrylonitrile (PAN) and polystyrene (PS) forming a continuous styrene-acrylonitrile phase (SAN), and butadiene constituting a dispersed polybutadiene rubber phase.

Figures 1b and c and Figures 2a and b report the spectral data obtained on the unaged LEGO by the multi-technique approach, here proposed, and aimed at probing the

1
2
3 mechanochemical properties of the ABS plastic combining integrated Brillouin and Raman
4 microspectroscopy, noninvasive external IR reflection spectroscopy (Figures 1b and c), and
5 unilateral NMR relaxometry (Figures 2a and b).
6
7

8 **[Insert Figure 1]**
9

10 Raman and IR spectroscopies enable the selective identification of the three polymer
11 components: PB, PS, and PAN^{3,25} (Figures 1b and c). Notably, the external reflectance spectrum
12 of ABS is mainly characterized by derivative-like bands due to a predominant Fresnel-type
13 reflection.³ In both mid-IR and Raman spectra, the predominant features are those of PS. In
14 Raman spectroscopy, PS is identified by the modes associated with the benzene ring: $\nu_s(\text{C}-\text{C})$ at
15 1602 cm^{-1} , $\nu_{as}(\text{C}-\text{C})$ at 1587 cm^{-1} , and 1449 cm^{-1} . Additionally, two intense peaks can be
16 observed at 1002 and 1032 cm^{-1} , due to the benzene ring breathing, and $\delta(\text{CH})$ in-plane of
17 benzene, respectively. Similarly, in IR spectroscopy, PS is identified by the signals associated
18 with the aromatic moiety, i.e., the characteristic stretching of the aromatic group $\nu(\text{CH})_{\text{Ar}}$ above
19 3000 cm^{-1} , the in-plane ring breathing modes (C=C stretching) at about 1600 cm^{-1} , the C=C
20 stretching vibrations of the aromatic ring at 1450 and 1490 cm^{-1} , the in-plane and out-of-plane
21 C-H bending at 1069 and 1028 cm^{-1} , and at 706 and 760 cm^{-1} , respectively. PB is identified in
22 the Raman spectrum by the band at around 1653 and 1668 cm^{-1} due to the $\nu(\text{C}=\text{C})$ cis and
23 trans,³⁵ respectively (that result in our profiles as a convoluted signal positioned at about 1670
24 cm^{-1}), and in the IR spectrum by the band at 965 cm^{-1} assigned to $\delta(\text{CH})_{\text{trans}}$. The bands
25 associated to the $\delta(\text{CH})_{\text{vinyl}}$ and $\delta(\text{CH})_{\text{cis}}$ of alkenes of PB at 911 and 736 cm^{-1} , respectively,
26 overlap with PS bands and are not considered in the present study.⁷ Finally, the nitrile group in
27 PAN can be clearly distinguished in both the Raman and IR spectra by the $\nu(\text{C}\equiv\text{N})$ at about 2240
28 cm^{-1} . The extended operative spectral range of external reflection IR spectroscopy, including the
29 near IR region (Figure 1c), mainly SWIR $6500\text{--}4000\text{ cm}^{-1}$; $1500\text{--}2500\text{ nm}$ provides further
30 information through detection of the combination and overtone bands of the three ABS
31 components probed at the subsurface of the samples.³ Within this range, notable bands
32 associated with PS are present, including the combination of the bending and stretching of the
33 aromatic C-H ($\nu+\delta$) CH_{Ar} in the range $4700\text{--}4500\text{ cm}^{-1}$, the first overtone of the aromatic C-H
34 stretching $2\nu(\text{CH})_{\text{Ar}}$ at about 6000 cm^{-1} , and the first overtone of the aliphatic C-H stretching
35 $2\nu(\text{CH})$ at approximately 5800 and 5700 cm^{-1} (antisymmetric and symmetric, respectively). The
36
37
38
39
40
41
42
43
44
45
46
47
48
49
50
51
52
53
54
55
56
57
58
59
60

1
2
3 nitrile group is distinctly identified by bands at 5246 and 5140 cm^{-1} assigned to the combination
4 of the nitrile stretching with the antisymmetric and symmetric stretching of CH_3 $\nu(\text{C}\equiv\text{N})+$
5 $\nu_{\text{as}}(\text{CH})$ and $\nu(\text{C}\equiv\text{N})+ \nu_{\text{s}}(\text{CH})$, respectively. Finally, PB can be identified by the presence of a
6
7 band at 4480 cm^{-1} assigned to the combination of the stretching and bending $\text{C-H} (\nu+\delta)\text{CH}$.³
8
9

10 The opposite side of the spectral range, at very low wavenumber values (below 5 cm^{-1} , in
11 the range of the GHz), BLS enables to probe ABS elasticity and local viscosity by analyzing the
12 frequency position and width of the Brillouin peak. The former is associated with the velocity of
13 acoustic waves propagation, while the latter determines their attenuation. BLS has been
14 extensively employed to monitor the viscoelastic behavior of various molecular liquids and
15 polymeric systems during physical and chemical vitrification.^{29–30,36} Figure 1b shows the
16 averaged Brillouin spectrum of five–point measurements, simultaneously collected with the
17 Raman, on the surface of the control sample (unaged). The Brillouin spectrum shows the
18 presence of a mechanically homogeneous surface at the microscale, with a unique Brillouin peak
19 (I_{BLS}) centered around 14 GHz (0.47 cm^{-1}).
20
21
22
23
24
25
26
27

28 Unilateral NMR relaxometry can offer further insights into ABS mechanical properties
29 and relaxation within the millisecond temporal regime (Figure 2). By applying a low external
30 magnetic field to the magnet, profilometry and relaxation time measurements provide
31 information about the sample's molecular mobility. The study of spin-lattice (T_1) and spin–spin
32 (T_2) relaxation times reflects the dynamics of atomic nuclei within the material, providing
33 insights into its structural and mechanical properties.³⁷ In Figures 2a and b, the longitudinal
34 NMR relaxation decay of magnetization (T_1) and distributions of T_2 are reported. In ABS
35 samples for all the depths of acquisition, T_1 exhibits a bi-exponential pattern characterized by
36 two components: a component of approximately 40 ms and a slower one of roughly 300 ms
37 (Table I). According to previous literature data,³⁸ the longest T_1 ($T_{1\text{b}}$) reflects the relaxation of
38 the polystyrene component, while the shortest one ($T_{1\text{a}}$) corresponds to the polybutadiene
39 component in the interphase formed by chemically bonded PS and PB chains.
40
41
42
43
44
45
46
47

48 **[Insert Figure 2]**
49

50 In polymers, it is well established that achieving a complete averaging of dipolar
51 interactions needs both high-frequency motions and long-range, low-frequency motions that
52 encompass substantial sections of the polymer molecules. It is widely acknowledged that T_1
53 constraints such as permanent chemical cross-links and molecular entanglements significantly
54
55
56
57
58
59
60

influence these long-range motions and predominantly govern the spin–spin relaxation time T_2 , making T_2 a valuable parameter for investigating network formation and its changes.³⁷ Following this, in Figure 2b, the T_2 distributions obtained at depths of 0.4 mm and 1.7 mm in ABS are reported. The T_2 distribution exhibits slight variation along the thickness of the sample. To obtain representative values of the observable variations throughout the sample thickness, transverse relaxation (T_2) times were measured at various depths, ranging from 0.2 to 1.9 mm below the surface with a step of 0.1 mm. T_2 values were extrapolated by fitting the transverse relaxation decays, employing a third-degree exponential function characterized by the relaxation times T_{2a} , T_{2b} and T_{2c} , along with their respective normalized weights $W_a\%$, $W_b\%$, $W_c\%$ (Eq. 3)

$$f(t) = W_a e^{-\left(\frac{t}{T_{2a}}\right)} + W_b e^{-\left(\frac{t}{T_{2b}}\right)} + W_c e^{-\left(\frac{t}{T_{2c}}\right)} \quad (3)$$

$$\text{with } \sum_{i=1}^n W_i = 100\% \quad n = 3$$

Consequently, the relaxation times and their corresponding relative weights were averaged throughout the entire depth range (Table I). Three T_2 components were observed: a faster component (T_{2a}) with an average value of 0.15 ms, affecting most of the spins (55%); an intermediate component, T_{2b} , with a duration of 5 ms, impacting approximately 5% of protons; and a slower component with an average of 13 ms (T_{2c}), affecting around the 40% of protons. The faster component can be ascribed to the rigid part (solid-like) of the polymer, which is attributed to the polystyrene–butadiene interface or the inter-crosslinked units of the polybutadiene.^{39,40} The presence of the intermediate (T_{2b}) and longer (T_{2c}) relaxation times can be ascribed to the soft component (liquid-like) of the polybutadiene, mainly arising from the uncrosslinked segments and the chain ends, which are more or less mobile.⁴¹ Pentimalli et al.⁴⁰ suggested that these two components might also reflect the heterogeneity in the ratio between cis-1,4 and trans-1,4 isomers. Nevertheless, a precise contribution of the chain segments cannot be easily defined, as the calculation of correlation times for motions and the degree of anisotropy in segmental motion could only be directly performed through a theoretical analysis of the magnetization decay curve obtained under a homogeneous magnetic field.

Table I. Average T_1 and T_2 relaxation times (T_{1a} , T_{1b} , T_{2a} , T_{2b} , and T_{2c}) and relative weights ($W_a\%$, $W_b\%$, and $W_c\%$) extrapolated from the relaxation decay of longitudinal and transverse magnetization of ^1H from 0.2 to 1.9 mm depths for ABS in unaged LEGO samples.

Relative weights (%)		Relaxation time (ms)	
$W_{2a}\%$	55	T_{2a}	0.15 ± 0.02
$W_{2b}\%$	5	T_{2b}	2.0 ± 1.1
$W_{2c}\%$	40	T_{2c}	13 ± 2
$W_{1a}\%$	65	T_{1a}	38 ± 9
$W_{1b}\%$	35	T_{1b}	294 ± 88

Mechanochemical Monitoring of the Photochemical Ageing of ABS-Based LEGO Bricks

The proposed multimodal approach combines spectroscopic data exploring different wavenumber ranges and probes different length-scale interaction, time-scale relaxation dynamics, and different sample depths. The approach was used to investigate compositional and mechanical variations resulting from ABS photooxidation.

The ABS samples were subjected to different times of light exposure by a xenon lamp with an irradiance of $\Phi_0 = 60 \text{ W/m}^2$ for a total time of 437 h (corresponding to a total dose of 390 kJ/cm^2) and monitored through the previously described multimodal approach.

Figure 3a shows the BRaMS spectra collected on the surface of the samples subjected to different doses (kJ/cm^2). The BRaMS integrated approach clearly reveals that photodegradation causes a shift of the ABS Brillouin peak to higher frequencies, from 14.27 GHz to 15.09 GHz. This shift is consistent with an increase in the stiffness of the material and is associated with the decrease of the Raman $\nu(\text{C}=\text{C})$ band at 1668 cm^{-1} assigned to PB.

External reflection IR observes the same trend, indicating a decrease of the unsaturated bond content of the PB fraction which is monitored by the band at 965 cm^{-1} $\delta(\text{CH})$ of PB.^{3,6,7} The disappearance of this band corresponds to an abrupt shift of the BLS peak (Figures 3a and b). Notably, these changes are concurrent with an increase in the intensity of $\nu(\text{C}=\text{O})$ band at

1
2
3 approximately 1730 cm^{-1} in the IR spectra (Figure 3b), indicative of a progressive oxidation of
4 the material.

5
6
7 [Insert Figure 3]

8 The mechanochemical correlation of the ABS photo-induced changes can be better
9 appreciated in Figure 4, where the frequency shift of the Brillouin peak (representing the changes
10 of the visco-elastic properties) is plotted as a function of the dose along with the Raman bands
11 ratio $\nu(\text{C}=\text{C})_{\text{PB}}/\nu_{\text{S}}(\text{C}-\text{C})_{\text{PS}}$ (Figure 3a) and the IR bands ratio $\delta(\text{CH})_{\text{PB}}/\nu+\delta(\text{CH})_{\text{PB}}$ (Figure 3b),
12 both representing the consumption of PB unsaturation due to aging.

13
14
15
16
17 These results show a sudden increase of the BLS frequency shift between 11 and 40
18 kJ/cm^2 energy density values (green and light blue spectra in Figure 3). The values of the elastic
19 modulus (M) and the acoustic absorption per wavelength ($\alpha\lambda$) were derived by traditional
20 acoustic analysis of BLS (SM) and illustrated in Figures 4c and d). It is evident that, for
21 exposures exceeding $60\text{ kJ}/\text{cm}^2$, the elastic modulus undergoes a sudden change, approaching a
22 saturation plateau. This change reflects an approximately 18% increase in the system's stiffness
23 when ABS undergoes photodegradation (Figure 4c). The correspondence between such a
24 variation and the observation of PB double bond consumption through oxidation, followed by
25 cross-linking, suggests that this process is responsible for the loss of elasticity in the material.
26 Furthermore, comparing the trend of $\alpha\lambda(\omega_{\text{B}})$ during the aging of ABS to that found for PB during
27 a cooling process toward its arrested glassy state⁴⁴ (Figure 4d), a remarkable similarity can be
28 appreciated. This similar trend suggests that, on the picosecond timescale, the relaxation
29 behavior of PB as neat polymer and in polymer blends (as ABS) involves the same segment of
30 the molecule. In the PB cooling process, BLS was found to be sensitive to fast secondary
31 relaxations associated with local density fluctuations due to changes in the length scale induced
32 by conformational torsions of the $-\text{CH}_2-\text{CH}=\text{}$ bond of polybutadiene.^{42,43} In ABS
33 photodegradation, the acoustic damping is likely due to the depletion of double bonds resulting
34 from the oxidation process and cross-linking of PB.

35
36
37
38
39
40
41
42
43
44
45
46
47
48 The correlated BLS and IR trend as a function of the aging was validated by repeating the
49 experiment on another set of LEGO bricks (ID element 4165967), as reported in Figure S2
50 (Supplemental Material), and the Brillouin frequency shift evaluated from the two different sets
51 of LEGO bricks were compared in Figure S3 (Supplemental Material).

52
53
54
55 [Insert Figure 4]

1
2
3 The infrared study of aged ABS LEGO bricks enabled us to define a surface degradation
4 index (SDI) function (Figure 4b, black line) obtained using a one-phase exponential decay fitting
5 of the ratio between the integral values of the PB bands at 965 cm^{-1} $\delta(\text{CH})$ and at approximately
6 4480 cm^{-1} $(\nu+\delta)(\text{CH})$ as a function of the photon flux.
7
8
9

10 Figure S4 (Supplemental Material) reports a closer view of the spectral changes during
11 aging of the two IR bands used to define the SDI function: the decreasing and disappearance of
12 the derivative-like peak at 965 cm^{-1} which indicates the surface removal of the PB unsaturation
13 with photoaging, and the almost steady band in the NIR range of the unsaturated bonds of
14 unaffected PB in the bulk. At a dose of approximately 40 kJ/cm^2 the ABS surface is completely
15 depleted of the PB unsaturation (Figure 4b; Figure S4, orange line), whilst the NIR band is still
16 visible and almost unchanged after 115 kJ/cm^2 (200h) of exposure (Figure 4b; Figure S4). Only
17 at the maximum tested dose, namely 390 kJ/cm^2 , the $(\nu+\delta)(\text{CH})$ combination band is slightly
18 shifted indicating that the amount of photo-aged ABS has reached a depth impacting the NIR
19 profiles, also in agreement with the NMR results which indeed indicates an involved thickness of
20 the first approximately 400 μm (Figure 5).
21
22
23
24
25
26
27
28

29 In the millisecond temporal regime, as expected NMR relaxometry reveals that
30 photochemical aging does not appear to significantly affect T_1 suggesting that the aging
31 primarily influences low-frequency motions (Figure S5, Supplemental Material). Conversely, the
32 study of T_2 is particularly useful for investigating changes in the mechanical properties of
33 materials. After photodegradation, i.e., after a 390 kJ/cm^2 of dose, a variation in the degree of
34 mobility can be observed following the decays of the transverse component of magnetization,
35 which is more sensitive to variations in microstructure, particularly local changes at different
36 depths (Figure S6, Supplemental Material). As an example, the comparison between the
37 distributions of T_2 measured at $400\text{ }\mu\text{m}$ depth before and after photochemical aging is reported in
38 Figure 5a. A slight decrease in the longer and intermediate T_2 relaxation times (T_{2b} and T_{2c}) is
39 observed, accompanied by a net increasing of protons density (Wa%) in the solid-like domain of
40 mobility, and a reduction of protons density in the mobile domain of mobility related to the soft
41 part of the polymer. As the solid-like fraction corresponds to protons in the crosslinked units of
42 polybutadiene, an increase in this fraction consequently indicates an increase in the cross-linking.
43 To evaluate the effect of the photochemical degradation along the thickness of the ABS, the
44 average relaxation time $1/\langle 1/T_2 \rangle$ as a function of the measurement depth is shown in Figure 5b.
45
46
47
48
49
50
51
52
53
54
55
56
57
58
59
60

1
2
3 Data show a reduction of the average relaxation times value after photoaging, evidencing a
4 difference until 600 μm of depth. Comparing the weights of the fast and slow components of T_2
5 (representing the fraction of solid-like domain of mobility- $W_a\%$ and the soft fraction of the
6 polymer- $W_c\%$) as function of the measured depths, a significant reduction in the soft fraction
7 mostly at the surface is observed (Figures 5c and d). The overall results suggest that after aging,
8 the majority of ^1H protons at the surface are involved in inter-crosslinked unit motions
9 contributing to an increase of the rigidity of the system. Within the first 200 μm of the sample,
10 data show that 98% of protons are in the solid-like domain of mobility, indicating that the mobile
11 fraction of the polymer is mostly lost. At deeper depths of 400 μm , the mobile fraction
12 progressively returns to the value found before the photoaging.
13
14

15
16
17
18
19
20 [Insert Figure 5]
21

22 Extensive research in the literature has established that the photo-oxidation of ABS
23 begins with a proton loss on the allylic position of the methylene group triggering the formation
24 of radicals.⁷ These radicals subsequently interact with oxygen, leading to the generation of oxo
25 and peroxy radicals within the polymer matrix. This oxidative process eventually results in the
26 introduction of carbonyl and hydroxyl functional groups into the polymer structure, attested by
27 the increase of the band in the $\nu(\text{C}=\text{O})$ region at approximately 1800–1600 cm^{-1} in the IR spectra
28 (Figure 2b). The photo-oxidative reactions occur on the polybutadiene component, remarked by
29 the decrease of the PB bands in the IR and Raman spectra (Figure 2). The newly formed alkyl
30 radicals also promote cross-linking reactions among PB chains (through C–C bridges) which
31 explains the stiffening of the surface of the ABS aged samples as detected by probing both the
32 relaxations at the ps (BLS) and ms (NMR relaxometry) time-scales.
33
34
35
36
37
38
39
40
41
42

43 *Mechanochemical Study of ABS-Based Design Objects*

44 Knowledge and outcomes of the photochemical study on LEGO bricks were exploited to study
45 ABS-based objects conserved at the Kartell Museum and the Italian Design Museum.
46
47

48 A total of 65 items were noninvasively investigated by external reflection spectroscopy in
49 the mid- and near infrared range, ABS was found in eighteen objects revealing an occurrence of
50 almost 30%. Among the ABS-based items, the majority is characterized by the absence of the PB
51 band at 965 cm^{-1} $\delta(\text{CH})$ indicating that the oxidative process has started and affected at least the
52
53
54
55
56
57
58
59
60

1
2
3 near surface (first micrometers). **<AUTHOR>Please note that the journal does not use**
4 **microns; micrometers was used instead.</AUTHOR>**
5

6
7 Figure 6 reports the infrared spectra recorded on the ABS-based items of the Kartell
8 Museum compared with spectra recorded on two LEGO bricks exposed to 11.2 and 390 kJ/cm²
9 of light (light green lines). In the iconic object of the Kartell Museum collection, the
10 “Componibile” colored modular unit (the round variants introduced in 1969, no. 4955), the
11 identification of ABS is achieved by observing the combined presence of bands associated to PS,
12 PAN and PB (Figure 6, red line). The latter is represented by the weak band at approximately
13 4480 cm⁻¹, indeed the signal at 965 cm⁻¹ is absent, suggesting a surface depleted of the
14 unsaturated PB moieties. These compositional details have been integrated with the mechanical
15 ones by NMR measurements on the same object. Relaxometry reveals an increased rigidity up to
16 800 μm, with a trend similar to that observed in the photo-aged LEGO (at maximum dose,
17 Figures 5c and d) although with different offset values that are linked to an original different
18 ABS mobility/rigidity (connected to the ABS polymer blend composition, additives, pigments,
19 and original structural/morphological properties). In addition, there is a notable decrease in the
20 mobile fraction, reaching a low average value around 10% in contrast to the 40% observed in the
21 LEGO sample (Figures 5c and d, gray line). The presence of a minor amount of the mobile
22 fraction in Componibile-4955 may be correlated with both differences of object intrinsic
23 properties (compositional, morphological) with respect to the bricks as well as a more
24 pronounced photodegradation.
25
26
27
28
29
30
31
32
33
34
35
36

37 **[Insert Figure 6]**
38

39
40 Assuming light as the main external factor of ABS degradation,^{3,4,6,8,10} and excluding
41 other intrinsic factors (not considered in the present model), the IR spectral data (Figure 6,
42 partially published in Rosi et al.³) were used to estimate the light dose received by two objects
43 conserved at the Italian Design Museum (Grillo Telephone, 0061, and Divisumma, 0331, Figure
44 S1) using the SDI function determined by the photo degradation model developed on the LEGO
45 bricks (Figure 4b, white circles and orange hexagons; Table II). These values were, then, used to
46 estimate the relative percentage variation of the Brillouin frequency shift (ν) and the elastic
47 modulus (M), related to the viscoelastic properties of the two objects, using the fitting relation
48 reported in Figure 4a (red line). Results are detailed in Table II. In the Grillo Telephone, point
49 0061_M_01, lacking the PB band in the mid-IR (Figure 6, grey line), shows an SDI value of 0,
50
51
52
53
54
55
56
57
58
59
60

1
2
3 corresponding to a light dose higher than 50 kJ/cm² (the threshold above which PB is no more
4 visible at the near surface) with a percentage of elastic deformation (with respect to the unaged
5 LEGO bricks) higher than 19%. The other spectra recorded on the Grillo are instead
6 characterized by variable SDI values leading to a light dose ranging from approximately 27 to 20
7 kJ/cm² with a percentage of the elastic deformation of 7.5%–10.0%. Table II also shows the
8 results obtained for the historical calculator Divisumma characterized by a higher SDI (according
9 to IR results, Figure 6, olive-green line) corresponding to an elastic deformation percentage of
10 10.

11
12
13
14
15
16
17
18
19 **Table II.** IR spectral data used to estimate the light dose received by the two objects conserved
20 at the Italian Design Museum using the SDI function determined by the photo degradation model
21 developed on the LEGO bricks. **<AUTHOR>Because there is not supplied title for Table II, a**
22 **shortened version of the paragraph above was used instead. Please correct, as**
23 **necessary.</AUTHOR>**

Sample name	SDI	Estimated total energy (kJ/cm ²)	BLS % of elastic deformation	
			v	M
0061_M_01	0	>50	appr 15.51 (9%)	appr 7.72(19%)
0061_M_02	1.69	26.71	14.88 (4.69%)	7.10 (9.3%)
0061_M_03	3.12	22.25	14.80 (4.11%)	7.02 (8.2%)
0061_M_05	4.26	19.97	14.75 (3.78%)	6.98 (7.5%)
0061_M_06	2.83	22.97	14.81 (4.21%)	7.03 (8.3%)
0331_M_03	1.25	28.91	14.92 (4.96%)	7.14 (10%)

44 45 Conclusion

46 A multimodal spectroscopic approach based on external reflection IR spectroscopy and NMR
47 relaxometry combined with correlative Brillouin and Raman microspectroscopy is presented to
48 monitor the photodegradation of ABS, with the dual aim of: (i) correlating the mechanical and
49 chemical modifications occurring at the material surface and subsurface at the microscale, and
50 (ii) increase the information we can provide from in situ noninvasive studies of museum objects
51
52
53
54
55
56
57
58
59
60

1
2
3 beyond polymer identification using coupling techniques available only in laboratories with
4 portable ones.
5

6 To achieve this, we performed a systematic study on laboratory models, conceiving a
7 photoaging model constructed using a combined mechanochemical study, and then applied it to
8 data acquired non-invasively on site.
9

10 The mechanochemical analysis enabled to experimentally correlate the photo-oxidative
11 reactions occurring on polybutadiene phase to the stiffening of the surface of the ABS aged
12 samples observed both in the ms and ps temporal regime. We further showed that the secondary
13 relaxations of ABS, assigned to conformational changes of the $-\text{CH}_2-\text{CH}=\text{}$ bonds of the
14 polybutadiene backbone, are like that observed for neat polybutadiene. In the ps time scale, PB,
15 as pure polymer and in polymer blends (such as ABS), behaves similarly. Further investigations
16 are necessary to confirm this intriguing finding, which will enable us to extend the photo-aging
17 model here proposed to other PB-containing plastics.
18
19

20 The photo-aging model allowed us to define a surface degradation index function to
21 estimate the state of conservation of ABS and to relate it to an equivalent light dose exposure. In
22 turn, this corresponds to a percentage of elastic deformation change that can be estimated from
23 the data acquired non-invasively by IR and NMR applied on-site. This result greatly impacts the
24 increase of the information we can provide by coupling techniques available only in laboratories
25 with portable techniques for the study of unique artistic objects, not sampleable. Furthermore, the
26 sensitivity of the analytical methods employed here to the surface properties can reveal early
27 photodegradation conditions that otherwise may remain unobserved by conventional surveys.
28 This aspect is crucial in defining on-time conservation strategies and correct displaying
29 environments.
30
31
32
33
34
35
36
37
38
39
40
41
42
43

44 **Acknowledgments**

45 This work was funded by the project Perspective- Piano Nazionale Di Ripresa E Resilienza
46 (PNRR) Missione 4 “Istruzione e Ricerca”–Componente C2 Investimento 1.1, “Fondo per il
47 Programma Nazionale di Ricerca e Progetti di Rilevante Interesse Nazionale (PRIN)” ID project
48 2022HSKH5Y Next Generation EU. We also acknowledge the European Union–
49 NextGenerationEU under the Italian Ministry of University and Research (MUR) National
50 Innovation Ecosystem grant ECS00000041–Vitality. Cup: B43C22000470005 and
51
52
53
54
55
56
57
58
59
60

J97G22000170005 for the support. Access to the MOLAB platform of the Italian node of the European Research Infrastructure for Heritage Science (www.erihs.it) has been funded by MUR through FOE E-RIHS 2022.

Supplemental Material

All supplemental material mentioned in the text is available in the online version of the journal.

References **<COPYEDIT/TYPESET>The REFERENCES have been checked and are already in ASP journal format. Cited journals without issue numbers as listed have never had issue numbers. PLEASE RETAIN THE NAMES AS LISTED IN THE REFERENCES: FIRST INITIAL, SURNAME.—Managing Editor </COPYEDIT/TYPESET>**

1. J.S. Martin, J.M. Cardamone, M.T. Baker. “Historic Textiles, Papers, and Polymers in Museums”. *J. Am. Inst. Conserv.* 2002. 41(1): 102–103. 10.2307/3179903
<AUTHOR>Ref. 1 is a review of the book "Historic Textiles, Papers, and Polymers in Museums". Is this correct or did you mean to cite the book instead?</AUTHOR>
2. B. Varghese, S. Schlick. “Microphase Separation in Poly(Acrylonitrile–Butadiene–Styrene) (ABS) Studied with Paramagnetic Spin Probes. I. Electron Spin Resonance Spectra”. *J. Polym. Sci., Part B: Polym. Phys.* 2002. 40(5): 415–423. 10.1002/polb.10110
3. F. Rosi, C. Miliani, P. Gardner, A. Chieli, et al. “Unveiling the Composition of Historical Plastics Through Non-Invasive Reflection FT-IR Spectroscopy in the Extended Near- and Mid-Infrared Spectral Range”. *Anal. Chim. Acta.* 2021. 1169: 338602. 10.1016/j.aca.2021.338602
4. D. Saviello, E. Pouvet, L. Toniolo, M. Cotte, A. Nevin. “Synchrotron-Based FTIR Microspectroscopy for the Mapping of Photo-Oxidation and Additives in Acrylonitrile-Butadiene-Styrene Model Samples and Historical Objects”. *Anal. Chim. Acta* 2014. 843: 59–72. 10.1016/j.aca.2014.07.021
5. C. Coon, B. Pretzel, T. Lomax, M. Strlič. “Preserving Rapid Prototypes: A Review”. *Herit. Sci.* 2016. 4: 40. 10.1186/s40494-016-0097-y
6. M. San Andrés, R. Chércoles, E. Navarro, J.M. de la Roja, et al. “Use of 3D Printing PLA and ABS Materials for Fine Art. Analysis of Composition and Long-Term Behaviour of Raw

- 1
2
3 Filament and Printed Parts”. *J. Cult. Herit.* 2023. 59: 181–189.
4 10.1016/j.culher.2022.12.005
5
6
7 7. R.M. Santos, G.L. Botelho, A.V. Machado. “Artificial and Natural Weathering of ABS”. *J.*
8 *Appl. Polym. Sci.* 2010. 116(4): 2005–2014. 10.1002/app.31663
9
10 8. D. Saviello, L. Andena, D. Gastaldi, L. Toniolo, et al. “Multi-Analytical Approach for the
11 Morphological, Molecular, and Mechanical Characterization After Photo-Oxidation of
12 Polymers Used in Artworks”. *J. Appl. Polym. Sci.* 2018. 135(17): 46194.
13 10.1002/app.46194
14
15 9. C. Freymond, X. Mackré-Delannoy, A. Guinault, C. Charbuillet, et al. “Thermal Oxidation of
16 Acrylonitrile-Butadiene-Styrene: Origin of the Ductile/Brittle Transition”. *Polym.*
17 *Degrad. Stab.* 2022. 206: 110–186. 10.1016/j.polymdegradstab.2022.110186
18
19 10. D. Comelli, F. Toja, C. D'Andrea, L. Toniolo, et al. “Advanced Non-Invasive Fluorescence
20 Spectroscopy and Imaging for Mapping Photo-Oxidative Degradation in Acrylonitrile–
21 Butadiene–Styrene: A Study of Model Samples and of An Object from the 1960s”.
22 *Polym. Degrad. Stab.* 2014. 107: 356–365. 10.1016/j.polymdegradstab.2013.12.030
23
24 11. F. Sabatini, S. Pizzimenti, I. Bargagli, I. Degano, et al. “A Thermal Analytical Study of
25 LEGO Bricks for Investigating Light-Stability of ABS”. *Polymers.* 2023. 15(15): 3267.
26 10.3390/polym15153267
27
28 12. M. Lazzari, D. Reggio. “What Fate for Plastics in Artworks? An Overview of Their
29 Identification and Degradative Behaviour”. *Polymers (Basel).* 2021.13(6): 883.
30 10.3390/polym13060883
31
32 13. S. França de Sá, S. Marques da Cruz, M.E. Callapez, V. Carvalho. “Plastics that Made
33 History: The Contribution of Conservation Science for the History of the Portuguese
34 Plastics Industry”. *Conserv. Património.* 2020. 35: 85–100. 10.14568/cp2019017
35
36 14. J.G. Bokria, S. Schlick. ”Spatial Effects in the Photodegradation of Poly(Acrylonitrile-
37 Butadiene-Styrene): A Study by ATR-FTIR”. *Polymer.* 2002. 43(11): 3239–3246.
38 10.1016/S0032-3861(02)00152-0
39
40 15. R. Chércoles Asensio, M. San Andrés Moya, J.M. de la Roja, M. Gómez. “Analytical
41 Characterization of Polymers Used in Conservation and Restoration by ATR-FTIR
42 Spectroscopy”. *Anal. Bioanal. Chem.* 2009. 395(7): 2081–2096. 10.1007/s00216-009-
43 3201-2
44
45
46
47
48
49
50
51
52
53
54
55
56
57
58
59
60

16. M. Lazzari, A. Ledo-Suárez, T. López, D. Scalarone, et al. “Plastic Matters: An Analytical Procedure to Evaluate the Degradability of Contemporary Works of Art”. *Anal. Bioanal. Chem.* 2011. 399(9): 2939–2948. 10.1007/s00216-011-4664-5
17. M. Picollo, G. Bartolozzi, C. Cucci, M. Galeotti, et al. “Comparative Study of Fourier Transform Infrared Spectroscopy in Transmission, Attenuated Total Reflection, and Total Reflection Modes for the Analysis of Plastics in the Cultural Heritage Field”. *Appl. Spectrosc.* 2014. 68(4): 389–396. 10.1366/13-07199
18. J. Bell, P. Nel, B. Stuart. “Non-Invasive Identification of Polymers in Cultural Heritage Collections: Evaluation, Optimisation and Application of Portable FTIR (ATR and External Reflectance) Spectroscopy to Three-Dimensional Polymer-Based Objects”. *Herit. Sci.* 2019. 7(1): 95. 10.1186/s40494-019-0336-0
19. L. Toniolo, S. Goidanich, F. Casadio. “Non-Invasive Identification of Plastic Materials in Museum Collections with Portable FTIR Reflectance Spectroscopy: Reference Database and Practical Applications”. *Microchem. J.* 2016. 124: 868–877. 10.1016/j.microc.2015.07.016
20. C. Cucci, G. Bartolozzi, V. Marchiafava, M. Picollo, et al. “Study of Semi-Synthetic Plastic Objects of Historic Interest Using Non-Invasive Total Reflectance FT-IR”. *Microchem. J.* 2016. 124: 889–897. 10.1016/j.microc.2015.06.010
21. E.M. Angelin, S. França de Sá, I. Soares, M.E. Callapez, et al. “Application of Infrared Reflectance Spectroscopy on Plastics in Cultural Heritage Collections: A Comparative Assessment of Two Portable Mid-Fourier Transform Infrared Reflection Devices”. *Appl. Spectrosc.* 2021. 75(7): 818–833. 10.1177/0003702821998777
22. L. Cséfalvayová, M. Strlič, H. Karjalainen. “Quantitative NIR Chemical Imaging in Heritage Science”. *Anal. Chem.* 2011. 83(13): 5101–5106. 10.1021/ac200986p
23. K. Saeki, K. Funatsu, K. Tanabe “Discrimination of Poly(Vinyl Chloride) Samples with Different Plasticizers and Prediction of Plasticizer Contents in Poly(vinyl chloride) Using Near-Infrared Spectroscopy and Neural-Network Analysis”. *Anal. Sci.* 2003. 19(2): 309–312. 10.2116/analsci.19.309
24. M.N. Boyden, E.M. Kleist, C.K. Asztalos, T.M. Korter “Determination of the Polymer Composition of Mid-Twentieth Century Purses by Raman Spectroscopy”. *Heritage Sci.* 2022. 10(1): 101. 10.1186/s40494-022-00743-0

- 1
2
3 25. D. Reggio, D. Saviello, M. Lazzari, D. Iacopino. “Characterization of Contemporary and
4 Historical Acrylonitrile Butadiene Styrene (ABS)-Based Objects: Pilot Study for
5 Handheld Raman Analysis in Collections”. *Spectrochim. Acta, Part A*. 2020. 242:
6 118733.
7
8
9
10 26. E.M. Angelin, S. França De Sá, M. Picollo, A. Nevin, et al. “The Identification of Synthetic
11 Organic Red Pigments in Historical Plastics: Developing An in Situ Analytical Protocol
12 Based on Raman Microscopy”. *J. Raman Spectrosc.* 2021. 52(1): 145–158.
13 10.1002/jrs.5985
14
15 27. C. Kehlet, S. Nunberg, S. Alcala, J. Dittmer. “Nuclear Magnetic Resonance Analysis for
16 Treatment Decisions: The Case of a White Sculptural Environment by Louise Nevelson”.
17 *Microchem. J.* 2018. 137: 480–484. 10.1016/j.microc.2017.12.004
18
19 28. N. Proietti, V. Di Tullio, D. Capitani, R. Tomassini, M. Guiso. “Nuclear Magnetic
20 Resonance in Contemporary Art: The Case of 'Moon Surface' by Turcato”. *Appl. Phys.*
21 *A*. 2013. 113(4): 1009–1017. 10.1007/s00339-013-7729-9
22
23 29. M. Alunni Cardinali, L. Cartechini, M. Paolantoni, C. Miliani, et al. “Microscale
24 Mechanochemical Characterization of Drying Oil Films by In Situ Correlative Brillouin
25 and Raman Spectroscopy”. *Sci. Adv.* 2022. 8(26): eabo4221. 10.1126/sciadv.abo4221
26
27 30. F. Scarponi, S. Mattana, S. Corezzi, S. Caponi, et al. “High-Performance Versatile Setup for
28 Simultaneous Brillouin-Raman Microspectroscopy”. *Phys. Rev. X*. 2017. 7(3): 031015.
29 10.1103/PhysRevX.7.031015
30
31 31. M. Alunni Cardinali, A. Di Michele, M. Mattarelli, S. Caponi, et al. “Brillouin–Raman
32 Microspectroscopy for the Morpho-Mechanical Imaging of Human Lamellar Bone”. *J. R.*
33 *Soc. Interface*. 2022. 19(187): 20210642. 10.1098/rsif.2021.0642
34
35 32. European Research Infrastructure for Heritage Science (E-RIHS). <https://www.e-rihs.eu/>
36 [accessed Jun 24 2024].
37
38 33. P.R. Griffiths, J.A. De Haseth. “Specular Reflection”. In: *Fourier Transform Infrared*
39 *Spectrometry*. Hoboken, New Jersey: John Wiley and Sons, Inc., 2007. Chap. 13, Pp.
40 277–300.
41
42 34. J. Perlo, F. Casanova, B. Blümich. “Profiles with Microscopic Resolution by Single-Sided
43 NMR”. *J. Magn. Reson.* 2005: 176(1): 64–70. 10.1016/j.jmr.2005.05.017
44
45
46
47
48
49
50
51
52
53
54
55
56
57
58
59
60

- 1
2
3 35. G. Bikulčius, I. Ignatjev, A. Ručinskienė. “Rapid Method to Determine Suitability of ABS
4 Plastics for Metallisation”. *Trans. IMF*. 2013. 92(1): 47–51.
5
6 10.1179/0020296713Z.000000000138
7
- 8 36. L. Comez, C. Masciovecchio, G. Monaco, D. Fioretto. "Progress in Liquid and Glass Physics
9 by Brillouin Scattering Spectroscopy". In: R.E. Camley, R.L. Stamps, editors. *Solid State
10 Physics*. Oxford: Academic Press, 2011. Chap. 1, Pp. 1–77. 10.1016/B978-0-12-397028-
11 2.00001-1
12
13
14
- 15 37. D.W. McCall. “Relaxation in Solid Polymers”. In: R.S. Carter, J.J. Rush, editors. *Special
16 Publication 301*. Washington, DC: U.S. Government Printing Office, 1969. Pp. 475–538.
17
18
- 19 38. Z. Yan, R. Zhang. “Measurement of Spin-Lattice Relaxation Times in Multiphase Polymer
20 Systems”. *J. Magn. Reson.* 2023. 357: 107597. 10.1016/j.jmr.2023.107597
21
- 22 39. F. Vilaplana, S. Karlsson, A. Ribes-Greus, C. Schade, et al. “NMR Relaxation Reveals
23 Modifications in Rubber Phase Dynamics During Long-Term Degradation of High-
24 Impact Polystyrene (HIPS)”. *Polymer*. 2011. 52(6): 1410–1416.
25
26 10.1016/j.polymer.2011.02.005
27
28
- 29 40. M. Pentimalli, D. Capitani, A. Ferrando, D. Ferri, et al. “Gamma Irradiation of Food
30 Packaging Materials: An NMR Study”. *Polymer*. 2000. 41(8): 2871–2881.
31
32 10.1016/S0032-3861(99)00473-5
33
- 34 41. G. Simon, H. Schneider, K.-G. Häusler. “¹H-NMR Transversal Relaxation in Crosslinked
35 1,4-*cis*-Polybutadiene”. In: I. Chudáček, editor. *Relationships of Polymeric Structure and
36 Properties*. Darmstad; New York: Steinkopff; Springer, 1998. Pp. 30–32.
37
38 10.1007/BFb0114341
39
40
- 41 42. A. Aouadiy, M.J. Lebony, C. Dreyfusy, B. Strubez, et al. “A Light-Scattering Study of 1-4
42 *cis-trans* Polybutadiene”. *J. Phys.: Condens. Matter*. 1997. 9(18): 3803–3820.
43
44 10.1088/0953-8984/9/18/018
45
- 46 43. D. Fioretto, C. Masciovecchio, M. Mattarelli, G. Monaco, et al. “Brillouin Light and X-ray
47 Study of Glass-Forming Polybutadiene”. *Philos. Mag. B*. 2002. 82(3): 273–281.
48
49 10.1080/13642810208221306
50
- 51 44. Y.Y. Huang, C.H. Wang. “Brillouin and Rayleigh Scattering in Polybutadiene”. *J. Chem.*
52 *Phys.* 1974. 61(5): 1868–1873. 10.1063/1.1682186
53
54
55
56
57
58
59
60

Figure Captions

Figure 1. (a) Images of ABS-based LEGO bricks and repeating units of PS, PB, and PAN; (b) BRaMS spectrum. (c) IR spectrum of ABS polymer along with peak assignments acquired from the unaged brick.

Figure 2. Unilateral NMR relaxometry analysis performed on the unaged LEGO: (a) Longitudinal relaxation decay of the ^1H with a constant time T_1 and (b) T_2 distributions measured at 0.4 and 1.7 mm depth.

Figure 3. (a) BRaMS and (b) IR spectra acquired from the LEGO samples during photoaging. Bands associated to butadiene are indicated and highlighted (PB) as well as the carbonyl stretching region $\nu(\text{C}=\text{O})$ to evidence the formation of oxidized species.

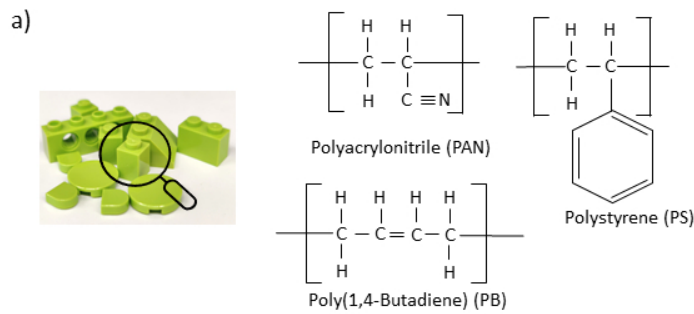
Figure 4. (a) Brillouin peak frequency shift values (red dots), $\nu(\text{C}=\text{C})_{\text{PB}}/\nu_{\text{S}}(\text{C}-\text{C})_{\text{PS}}$ Raman band ratio (blue squares) and (b) $\delta(\text{CH})_{\text{PB}}/(\nu+\delta)(\text{CH})_{\text{PB}}$ IR band ratio corresponding to the superficial and sub-superficial PB, respectively, as a function of the light dose. The black line represents the SDI function modelled for the LEGO samples (black dots). White circles and orange hexagon correspond to the plastic objects of the Italian Design Museum 0061 and 0331, respectively; (c) longitudinal elastic modulus (M) and (d) acoustic dissipation ($\alpha\lambda$) derived from BLS spectra of ABS, reported as a function of the photon flux (TE) normalized to the value corresponding to 60 kJ/cm^2 (TE^*) (present study, blue spheres); $\alpha\lambda$ for PB as a function of the temperature normalized to the glass transition temperature as published in Huang and Wang⁴⁴ is also reported (violet stars).

Figure 5. (a) Comparison between the distributions of T_2 measured at depths of 400 μm before and after photochemical aging; (b) average relaxation time $1/\langle 1/T_2 \rangle$ as a function of the depth of measurement before and after the aging; (c) protons solid-like fraction ($W_a\%$) as a function of the depth of measurements within ABS (black and red) before and after photodegradation and in the Kartell object Componibile-4955 (grey); (d) protons mobile fraction ($W_c\%$) as a function of the depth of measurements within ABS (black and red) before and after photochemical aging and

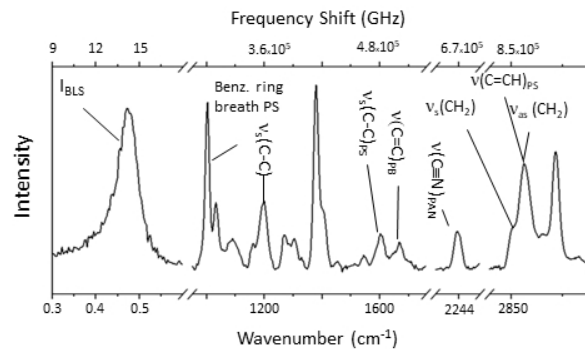
1
2
3 in a Kartell object Componibile-4955 (grey). Dashed lines indicate the best-fitting of data
4 obtained by a sigmoidal function.
5
6
7

8 **Figure 6.** IR spectra recorded from the ABS items of the Kartell Museum and Italian Design
9 Museum compared with spectra recorded on two LEGO bricks exposed to 11.2 and 390 kJ/cm²
10 of light (blue lines). Componibile-4955 (red line); Grillo Telephone-0061 (point 03 black line,
11 point 01 grey line); Divisumma-0331 (olive-green line).
12
13
14
15
16
17
18
19
20
21
22
23
24
25
26
27
28
29
30
31
32
33
34
35
36
37
38
39
40
41
42
43
44
45
46
47
48
49
50
51
52
53
54
55
56
57
58
59
60

Peer Review Version



b) Brillouin and Raman micro-spectroscopy



c) External reflection FT-IR

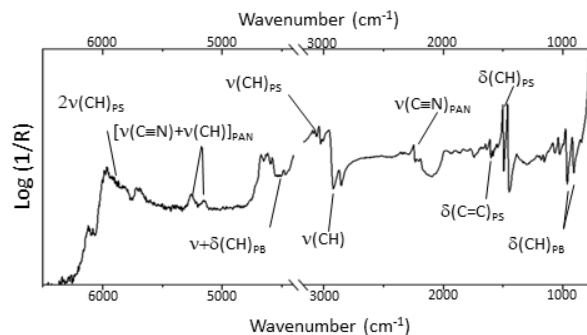


Figure 1 a) Images of ABS-based LEGO® bricks and repeating units of polystyrene-PS, polybutadiene-PB and polyacrylonitrile-PAN; b) BRaMS spectrum; c) IR spectrum of ABS polymer along with peaks assignment (PS = polystyrene, PB = polybutadiene, PAN = polyacrylonitrile, Ar = aromatic, v = stretching deformation, δ = bending deformation, s = symmetric, as = asymmetric) acquired on the unaged brick.

481x641mm (38 x 38 DPI)

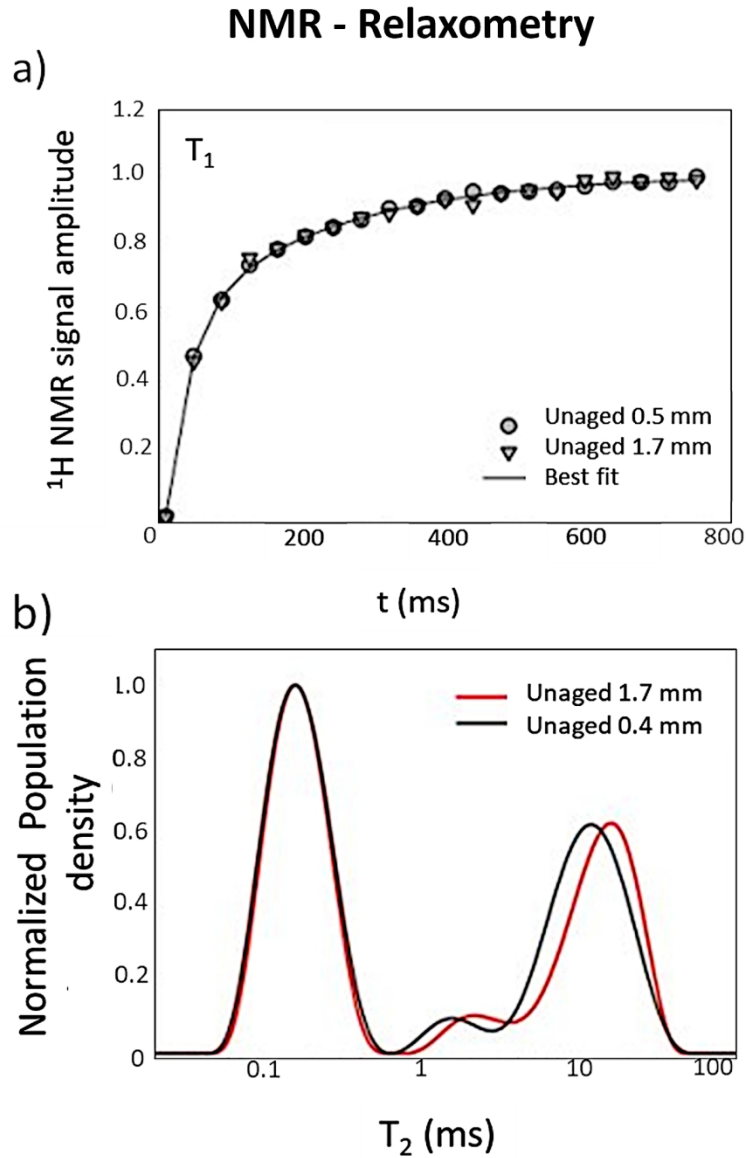


Figure 2 Unilateral NMR relaxometry analysis performed on the unaged LEGO® a) Longitudinal relaxation decay of the ^1H with a constant time T_1 ; b) T_2 distributions measured at 0.4 and 1.7 mm depth.

286x424mm (130 x 130 DPI)

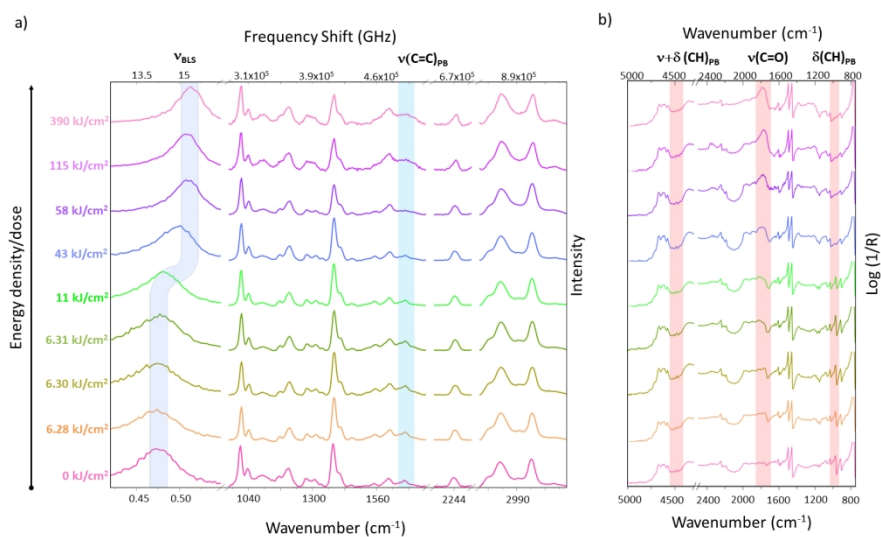


Figure 3 a) BRAMS and b) IR spectra acquired on the LEGO® samples during photoaging. Bands associated to butadiene are indicated and highlighted (PB) as well as the carbonyl stretching region $\nu(\text{C}=\text{O})$ to evidence the formation of oxidized species.

1235x695mm (38 x 38 DPI)

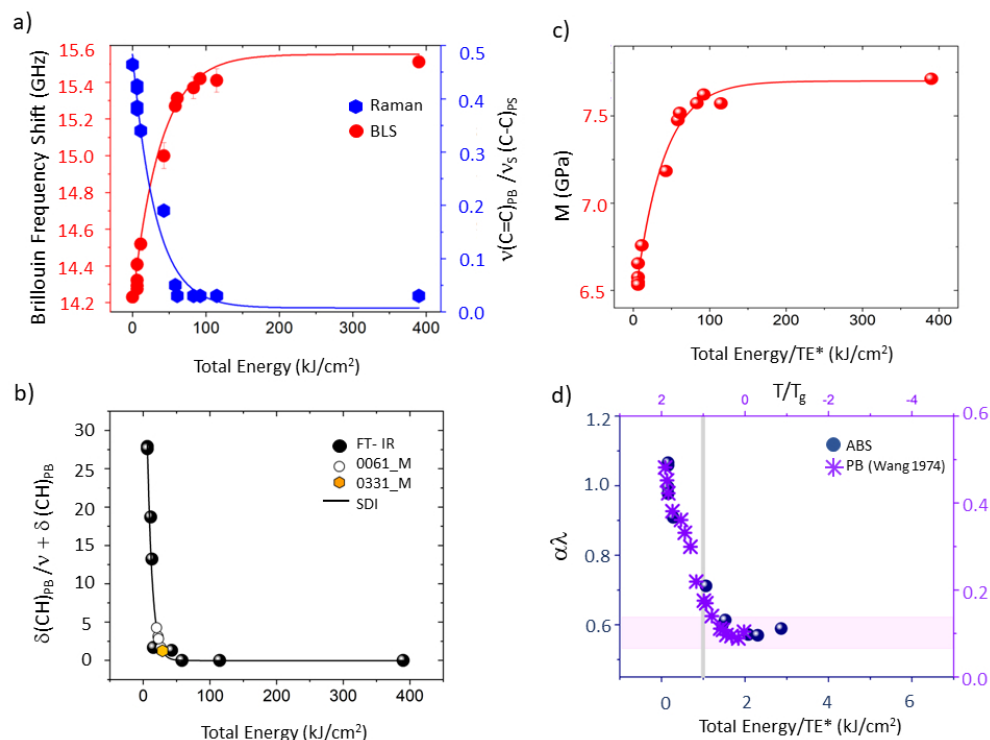


Figure 4. a) Brillouin peak frequency shift values (red dots), $\nu(\text{C}=\text{C})_{\text{PB}}/\nu_{\text{S}}(\text{C}-\text{C})_{\text{PS}}$ Raman band ratio (blue squares) and b) $\delta(\text{CH})_{\text{PB}}/(\nu + \delta)(\text{CH})_{\text{PB}}$ IR band ratio corresponding to the superficial and sub-superficial PB, respectively, as a function of the light dose. The black line represents the Surface Degradation Index (SDI) function modelled for the LEGO® samples (black dots). White circles and orange hexagon correspond to the plastic objects of the Italian Design Museum 0061 and 0331, respectively; c) longitudinal elastic modulus (M) and d) acoustic dissipation ($\alpha\lambda$) derived from BLS spectra of ABS, reported as a function of the photon flux (Total Energy) normalized to the value corresponding to 60 kJ/cm² (TE*) (present study, blue spheres); $\alpha\lambda$ for polybutadiene (PB) as a function of the temperature normalized to the glass transition temperature as published in Ref. 44 is also reported (violet stars, PB Wang1974).

641x481mm (38 x 38 DPI)

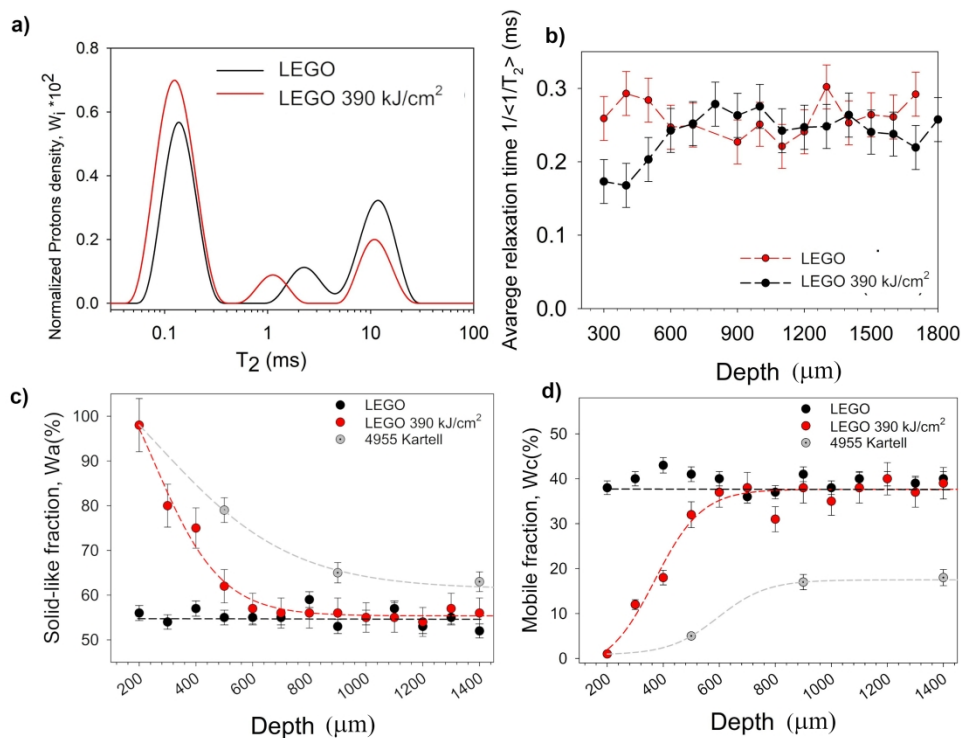


Figure 5. a) Comparison between the distributions of T_2 measured at depths of 400 μm before and after photochemical aging; b) average relaxation time $1/\langle 1/T_2 \rangle$ as a function of the depth of measurement before and after the aging; c) protons solid-like fraction (W_a %) as a function of the depth of measurements within ABS (black and red) before and after photodegradation and in the Kartell object Componibile-4955 (grey); d) protons mobile fraction (W_c %) as a function of the depth of measurements within ABS (black and red) before and after photochemical aging and in a Kartell object Componibile-4955 (grey). Dash lines indicate the best-fitting of data obtained by a sigmoidal function.

700x524mm (130 x 130 DPI)

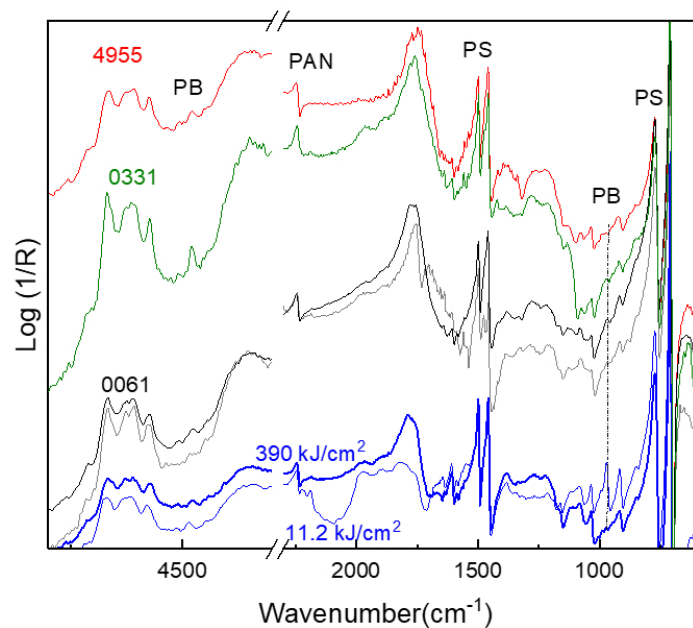


Figure 6. IR spectra recorded on ABS-items of the Kartell Museum and Italian Design Museum compared with spectra recorded on two LEGO® bricks exposed to 11.2 and 390 kJ/cm² of light (blue lines). Comonibile-4955 (red line); Grillo Telephone-0061 (point 03 black line, point 01 grey line); Divisumma-0331 (olive-green line). PB=polybutadiene; PS=polystyrene, PAN=polyacrylonitrile

641x481mm (38 x 38 DPI)

SUPPLEMENTAL MATERIAL

Assessing Mechanochemical Properties of Acrylonitrile Butadiene Styrene (ABS) Items in Cultural Heritage Through a Multimodal Spectroscopic Approach

Irene Bargagli^{1,2,#}, Martina Alunni Cardinali^{2,#}, Valeria Di Tullio³, Brenda Doherty¹, Marco Paolantoni², Daniele Fioretto^{4,5}, Noemi Proietti³, Francesca Sabatini^{1†}, Costanza Miliani⁶, Elisa Storace⁷, Sara Russo⁸, Rafaela Trevisan⁹, Alessandra Vannini⁹, Laura Cartechini^{1,*}, Lucia Comez^{5,*}, Francesca Rosi^{1,*}

authors contributed equally

¹ CNR, Istituto di Scienze e Tecnologie Chimiche “Giulio Natta” (SCITEC), via Elce di Sotto, 8 06123 Perugia, Italy

² Department of Chemistry, Biology and Biotechnology, University of Perugia via Elce di Sotto, 8 06123, Italy

³ CNR, Istituto di Scienze del Patrimonio (ISPC), Strada Provinciale 35d, n. 9, 00010, Montelibretti (Roma), Italy

⁴ Dipartimento di Fisica e Geologia Università di Perugia, via Pascoli 8 06123 Perugia

⁵ CNR, Istituto Officina dei Materiali (IOM), Via Pascoli, 06123 Perugia, Italy

⁶ CNR, Istituto di Scienze del Patrimonio (ISPC), Via Guglielmo Sanfelice, 8 80134 Napoli, Italy

⁷ Fondazione Museo Kartell, Via delle Industrie 3, 20082 Noviglio Milano, Italy

⁸ Università degli Studi di Firenze, Dipartimento di Storia, Archeologia, Geografia, Arte e Spettacolo, Via S. Gallo, 10-50129 Firenze, Italy

⁹ Triennale Milano, Conservazione e restauro, viale Emilio Alemagna 6, 20121 Milano, Italy

† Present address: Department of Earth and Environmental Sciences, University of Milano-Bicocca, Piazza della Scienza 1, 20126 Milan, Italy

*Corresponding author emails: laura.cartechini@cnr.it; comez@iom.cnr.it; francesca.rosi@cnr.it

HISTORICAL DESIGN OBJECTS

Figure S1 depicts the objects investigated in the present study, they belong to two internationally renowned design museums: the Italian Design Museum and the Kartell Museum.

The Italian Design Museum, inaugurated in 2007, is the first Italian design museum. It houses a wide collection of iconic objects (furniture, accessories, and electronics) dating from 1927 to the present day and represents the history of Italian design. The results presented here refer to the Grillo Phone-0061 and Divisumma-0336 (FigureS1).

The Kartell Museum was established in 1999 on the company's fiftieth anniversary by President Claudio Luti to conserve, promote and enhance the company's material and intangible cultural heritage. The display includes iconic objects of Italian design produced from the year of foundation of the company, 1949, to date. The results presented here refer to the Componibile-4955 (FigureS1).

TRADITIONAL ACOUSTIC ANALYSIS OF BLS DATA

The BLS spectra were analysed in the narrow region around the Brillouin peak following the procedure described in Ref. 1. The intensity of BLS doublets, I_B , was modelled using a damped harmonic oscillator (DHO) line shape (Eq. S1):

$$I_B(\omega) = I_0/\pi (\Gamma_B \omega_B^2)/(\omega_B^2 - \omega^2)^2 + (\omega \Gamma_B)^2 \quad (\text{Eq. S1})$$

where I_0 is an amplitude factor depending on the scattering cross-section, $v_B = \omega_B/2\pi$ and $\Gamma_B/2\pi$ denotes the frequency shift and the full width at half-maximum (FWHM) of the Brillouin peaks, respectively.

Specifically, ω_B and Γ_B are directly linked to the longitudinal elastic modulus, $M = \rho \omega_B^2/q^2$, and the acoustic absorption, $\alpha = q \Gamma_B/2\omega_B$, of the elastic wave propagating within the medium, respectively related to the material's stiffness and the ability to dissipate acoustic energy through relaxation channels. In the above, ρ is the mass density of the material, and q represents the exchanged wavenumber related to the incident wavelength, λ , the scattering angle θ , and the refractive index n of the medium, through the relation $q = (4\pi n/\lambda) \sin(\theta/2)$.

In the present experiment, vertically polarized scattered light was analysed in the backscattering geometry, so that $q = (4\pi n/\lambda)$, with $\lambda = 532$ nm. In a previous work on linseed oil polymerization², we demonstrated how variations in density and refractive index have very little influence on the overall trend of the moduli during the process of drying. Similarly, in this study, we calculated $M(\omega_B)$ and $\alpha\lambda(\omega_B)$ considering values of $n = 1.538^3$ and $\rho = 1.07$ g/cm³⁴ as constants assuming negligible their changes in the overall moduli variation during the photochemical aging.

REPRODUCIBILITY ACROSS DIFFERENT LEGO SERIES

The reproducibility of the photochemical ageing trend was tested using a second set of Lego bricks (ID element 4165967, see Materials and methods in the main paper). The Brillouin (left) and external reflection IR (right) spectra in Figure S2a), plotted as a function of the increased photon flux, show that photochemical ageing is again associated with an increase in the frequency shift of the Brillouin peak. Figure S2b) shows that the blue shift in the frequency value of the BLS peak (red) correlates with the decrease in the IR ratio between the $\delta(\text{CH})$ at 965 cm⁻¹/($\nu + \delta$)(CH) at 4480 cm⁻¹ modes of PB. It is worth noting that the abrupt increase in the maximum of the BLS peak occurs between energy density values of 14 and 42 kJ/cm², confirming that the loss of elasticity in the ABS plastic is due to the progressive degradation of the poly-butadiene rubber.

Notably, Figure S3 reports the Brillouin Frequency Shift from the two different sets of LEGO® bricks (year 2022-batch number 11019 and year 2023- ID element 4165967) reported as a function

of the light dose. The comparison clearly shows that not only the trend but also the absolute values of the frequency shift can be reproduced between the different sets.

FIGURES

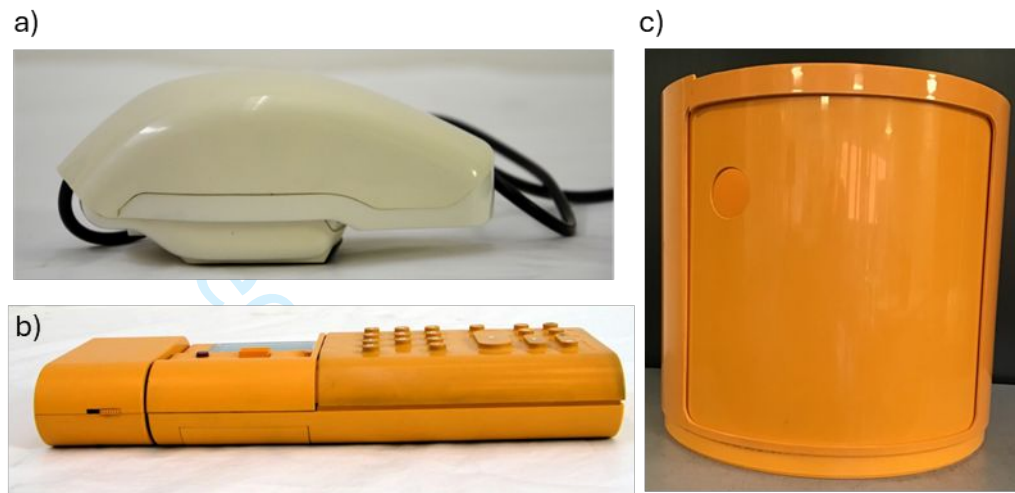


Figure S1. Historical objects belonging to a-b) Italian Design Museum: Grillo Telephone-0061 and Divisumma-0331, c) Kartell Museum Componibile-4955

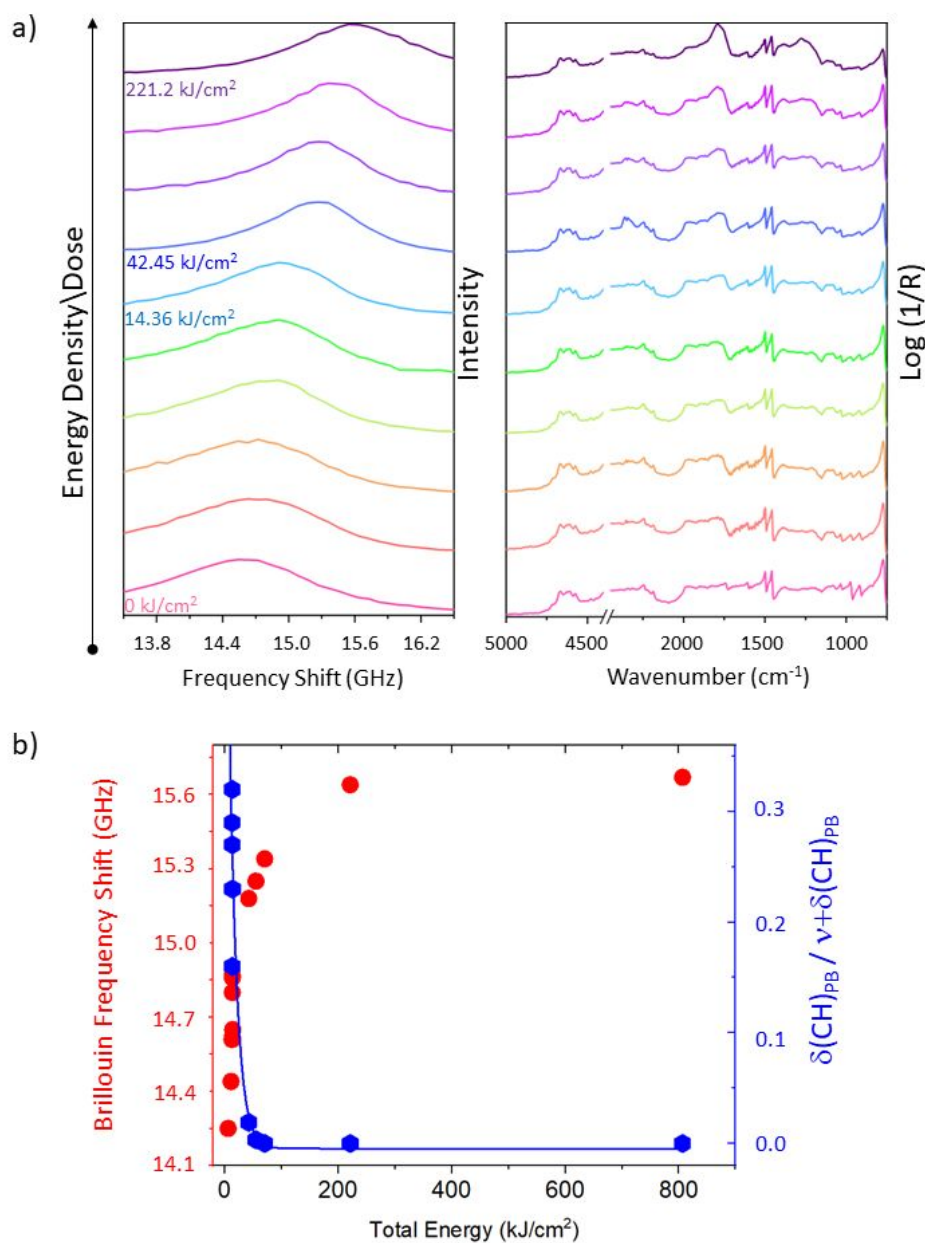


Figure S2. (a) Brillouin and FT-IR spectra acquired on a different set of LEGO bricks in lime green color samples (ID element 4165967), subjected to increasing photon flux. (b) Brillouin Frequency Shift (red circles) and the relative ratio between IR bands (blue hexagons), corresponding to the $\delta(\text{CH})_{\text{PB}}$ at 965 cm^{-1} and the $(\nu + \delta)(\text{CH})_{\text{PB}}$ as a function of the light dose.

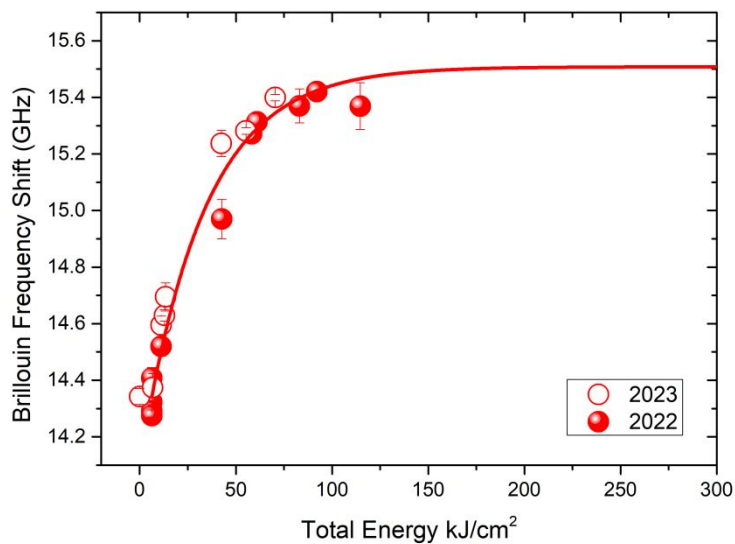


Figure S3. Brillouin Frequency Shift evaluated from two different sets of LEGO bricks (The Lego Group) in lime green colour, i.e., year 2022-batch number 11019 (solid circles) and year 2023-ID element 4165967 (open circles), reported as a function of the light dose.

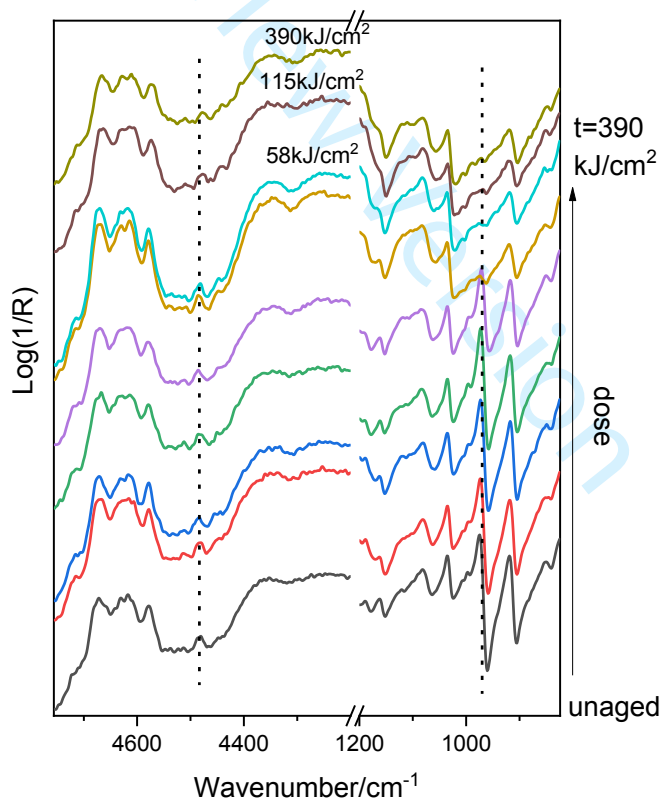


Figure S4. IR spectra, acquired in external reflection mode, recorded at increasing ageing doses with indicated the vibrational modes of polybutadiene- the $\delta(\text{CH})_{\text{PB}}$ at 965 cm^{-1} (superficial PB)

and the $(\nu+\delta)(\text{CH})_{\text{PB}}$ (sub-superficial PB)- considered for the definition of the surface degradation index (SDI) function.

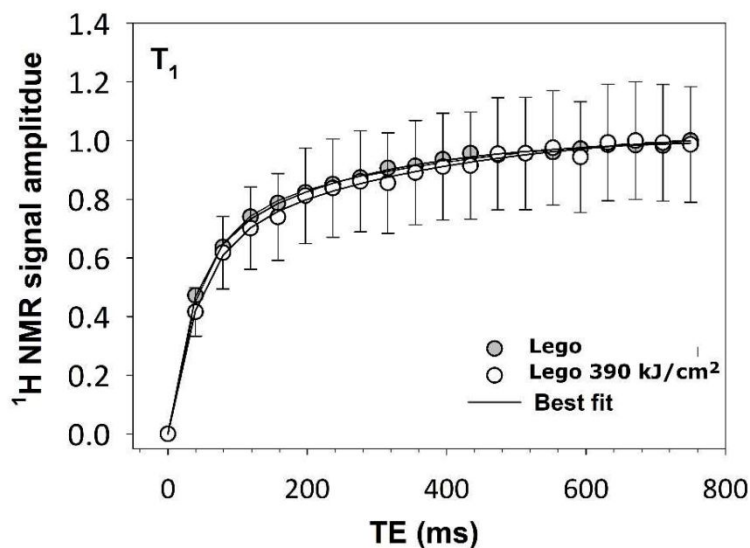


Figure S5. Comparison of the decays in the longitudinal magnetization component, T_1 , measured at depths of 400 μm before and after photochemical aging.

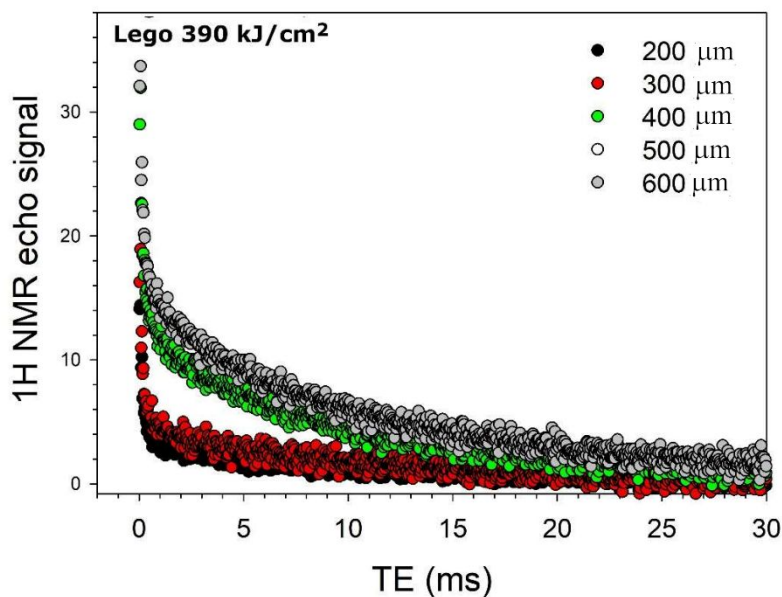
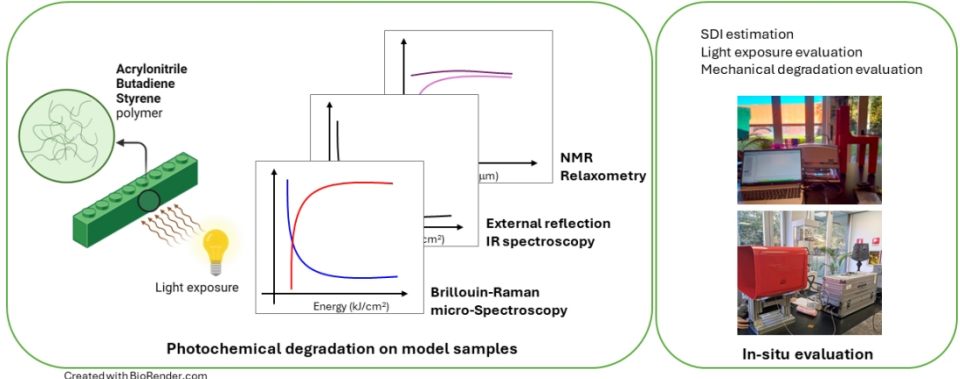


Figure S6. Comparison of the decays of the transverse magnetization component, T_2 , measured along the thickness of the LEGO sample aged with a dose of 390 kJ/cm^2 .

REFERENCES

1. L. Comez, C. Masciovecchio, G. Monaco, D. Fioretto. "Progress in Liquid and Glass Physics by Brillouin Scattering Spectroscopy". In: R.E. Camley, R.L. Stamps, editors. Solid State Physics. Oxford: Academic Press, 2011. Chap. 1, Pp. 1–77. 10.1016/B978-0-12-397028-2.00001-1
2. M. Alunni Cardinali, L. Cartechini, M. Paolantoni, C. Miliani, et al. "Microscale Mechanochemical Characterization of Drying Oil Films by In Situ Correlative Brillouin and Raman Spectroscopy". Sci. Adv. 2022. 8(26): eabo4221. 10.1126/sciadv.abo4221
3. Syntec Optics. <https://syntecoptics.com/optical-materials/> [accessed 24 June 2024].
4. PlasticRanger. "Density of ABS Material: The Complete Guide". <https://plasticranger.com/density-of-abs-material/> [accessed 24 June 2024].

1
2
3
4
5
6
7
8
9
10
11
12
13
14
15
16
17
18
19
20
21
22
23
24
25
26
27
28
29
30
31
32
33
34
35
36
37
38
39
40
41
42
43
44
45
46
47
48
49
50
51
52
53
54
55
56
57
58
59
60



855x481mm (38 x 38 DPI)